

Performance Analysis for Continuous Antennas in Rician Channels

Peter J. Smith, *Fellow, IEEE*, Erfan Khordad *Member, IEEE*,
Rajitha Senanayake, *Member, IEEE*, Justin P. Coon, *Senior Member, IEEE*

Abstract—Antenna arrays with discrete antenna elements have been conventionally used in multiple-input multiple-output (MIMO) communications. Improved spectral efficiency resulting from more antenna elements has motivated the idea of packing very large numbers of elements in an array, yielding continuous-like antennas. This paper conducts a performance analysis of continuous antennas, employing matched filtering. We derive a gamma approximation for the instantaneous received signal-to-noise ratio (SNR) under a Rician channel with a spatially-correlated non-line-of-sight (NLoS) component. We also derive the mean and an upper bound for achievable rate. Numerical results demonstrate the accuracy of our approximations across a range of parameters.

Index Terms—Continuous antenna, matched filtering.

I. INTRODUCTION

Antenna arrays have conventionally been modelled as a fixed arrangement of discrete antenna elements. However, this arrangement is challenged by several emerging trends such as fluid/movable antennas, super wideband massive MIMO, holographic MIMO etc. All these systems point towards an array packed with an extremely large number of antenna elements or a *continuous-like* antenna arrangement [1], [2].

Following these trends, it is now timely to consider the capability of devices with continuous spatial processing across the antenna aperture. Motivated by this, in this paper, we perform an analysis for continuous antennas, based on the assumption that signal processing occurs at all points on the continuous antenna. This theoretical exercise is crucial to understand the ultimate performance of such systems.

There has been progress in studying continuous antennas. Matched filtering (MF) was used in [3] to study the spatial degrees of freedom and capacity of a continuous surface system for different settings of users, considering an infinitely large surface and a line of sight (LoS) channel model. A finite dimension continuous surface was considered in [4], [5] with MF and the surface was split into sub-surfaces corresponding to single-antenna users. Assuming an infinite number of sub-surfaces, in [4], the uplink data rate of a sub-surface was analyzed. Also with the same assumption in [5], the uplink sum-rate distribution was approximated. In [6], capacity analysis was performed for a one-dimensional (1-D) continuous antenna, assuming a LoS channel model. Nonetheless, the approaches in [3], [6] ignored the spatial channel correlation and in [4], [5] only the correlation in the interference channel was considered. The spatial channel correlation across the continuous antenna needs to be considered for accurate performance analysis, as considered in [7], [8] for continuous antennas. As such, in [9] we considered a spatially

correlated Rayleigh channel across the continuous antenna and derived analytical expressions for performance measures.

In this paper, we extend the work in [9] to the more complete and more challenging case of Rician channels. We consider a single-antenna user communicating with a receiver having a finite-dimension continuous antenna and derive performance measures by employing MF, under a Rician channel model with a spatially-correlated NLoS component. We derive exact expressions for the mean SNR and SNR variance. Hence, we develop a gamma approximation for the instantaneous received SNR leading to outage results as well as approximations and a bound on achievable rate. We also present the 1-D continuous antenna as a special case. Our numerical results illustrate that our approximation for the SNR is an excellent fit, leading to accurate performance analysis across a range of system parameters.

This work is complementary to the important work in [8] on correlated Rician fading. In [8], the mutual information is modelled as Gaussian using the central limit theorem, for the limiting regime of infinitely large continuous antennas at both transmitter and receiver ends. The work in [8] has a complex channel model so that asymptotic results are required. Hence, we adopt a simpler, widely-used channel model so that some exact results and tight approximations are possible in the finite-dimensional case.

II. SYSTEM MODEL

We consider a receiver equipped with a continuous surface antenna with width W and height H and a single antenna user as a transmitter. The channel between the continuous antenna and the user is denoted by $h(x, y)$, with $0 \leq x \leq W$ and $0 \leq y \leq H$. The received signal at point (x, y) on the continuous antenna is given by

$$r(x, y) = h(x, y)s + n(x, y), \quad (1)$$

where $n(x, y)$ denotes the noise process and s is the transmit symbol with $\mathbb{E}[|s|^2] = E_s$. The noise process is zero-mean Gaussian with covariance structure $\mathbb{E}[n(x_1, y_1)n^*(x_2, y_2)] = \sigma^2 \rho(x_1, y_1, x_2, y_2)$ where the correlation function, $\rho(\cdot)$, satisfies $|\rho(x_1, y_1, x_2, y_2)| \leq 1$. We assume that the channel is a Rician process and is defined with Rician K-factor, κ , as

$$h(x, y) = \sqrt{\beta} \left(\sqrt{\frac{\kappa}{\kappa+1}} a(x, y) + \sqrt{\frac{1}{\kappa+1}} u(x, y) \right), \quad (2)$$

where $a(x, y)$ is the deterministic LoS component with $|a(x, y)| = 1$ and $u(x, y) \sim \mathcal{CN}(0, 1)$ denotes the NLoS component. $u(x, y)$ is a correlated Rayleigh process with correlation function $\mathbb{E}[u(x_1, y_1)u^*(x_2, y_2)] = c(x_1, y_1, x_2, y_2)$ where $|c(\cdot)| \leq 1$. β is the fixed channel gain for all (x, y) .

We assume that MF is performed at every point of the continuous antenna as in [3], [6]. The aggregated output over the continuous antenna is written as

$$Z = \int_0^H \int_0^W h^*(x, y) r(x, y) dx dy \triangleq \eta s + w, \quad (3)$$

where for ease of notation we have defined $\eta = \int_0^H \int_0^W |h(x, y)|^2 dx dy$ and $w = \int_0^H \int_0^W h^*(x, y) n(x, y) dx dy$. Hence, the instantaneous received SNR is

$$\gamma_s = E_s |\eta|^2 / \mathbb{E}_n [|w|^2]. \quad (4)$$

Next, we conduct a performance analysis of this system.

III. PERFORMANCE ANALYSIS

In this section, we derive an accurate gamma approximation for the SNR distribution by deriving an exact expression for the signal power. First we simplify the SNR expression in (4) by calculating the noise power as

$$\begin{aligned} \mathbb{E}_n [|w|^2] &= \int_0^H \int_0^H \int_0^W \int_0^W \mathbb{E}_n [h^*(x, y) h(x', y')] \mathbb{E}_n [n(x, y) n^*(x', y')] \\ &\quad dx dx' dy dy' \\ &= \sigma^2 \int_0^H \int_0^H \int_0^W \int_0^W h^*(x, y) h(x', y') \rho(x, y, x', y') dx dx' dy dy'. \end{aligned} \quad (5)$$

Simplification of (5) requires the noise correlation. For simplicity, we assume a spatially white noise process, so that $\rho(x_1, y_1, x_2, y_2) = \delta(|x_1 - x_2| + |y_1 - y_2|)$, where $\delta(\cdot)$ is the delta function. This gives $\mathbb{E}_n [|w|^2] = \sigma^2 \int_0^H \int_0^W |h(x, y)|^2 dx dy$. Substituting this noise power and η into (4), the instantaneous received SNR in (4) is written as

$$\gamma_s = \frac{E_s}{\sigma^2} \int_0^W \int_0^H |h(x, y)|^2 dy dx = \frac{E_s}{\sigma^2} \eta. \quad (6)$$

A. SNR Distribution

We now derive a gamma approximation for the distribution of γ_s in (6). Gamma approximations are used widely in communications theory as a tool for performance analysis when an intractable distribution is known to be non-negative, positively skewed and uni-modal. In particular, a gamma approximation is often very accurate when the underlying variable is a sum of positive random variables, such as chi-squared variables (e.g., [10]–[12]). The gamma approximation provides a tool for performance analysis of continuous antennas, with significantly smaller computational burden compared to simulations.

Note that $|h(x, y)|^2$ in (6) has a scaled non-central chi-squared distribution but the integral of a non-central chi-squared process does not have a known distribution. However, the integral is the limit of a sum and such sums can be accurately approximated by a gamma variable [10], [11]. Motivated by this, we approximate γ_s with a gamma random variable. We derive the first and second moments of γ_s to obtain the shape and scale parameters of the approximated gamma variable. Note that the gamma approximation is the first term in a Laguerre series expansion for the density. The accuracy of the approximation can be improved by deriving higher order moments and using more terms in the expansion

[11]. However, numerical results in Sec. IV show that our approximation using the first two moments is adequate.

We now proceed to compute the first and second moments of γ_s . We compute the first moment as:

$$\mathbb{E} [\gamma_s] = E_s \beta W H / \sigma^2, \quad (7)$$

which follows from $c(x, y, x, y) = 1$. As expected, the mean SNR is only a function of the area, $W \times H$, of the array and not the shape. The second moment is

$$\mathbb{E} [\gamma_s^2] = \frac{E_s^2}{\sigma^4} \int_0^H \int_0^H \int_0^W \int_0^W \mathbb{E} [|h(x, y)|^2 |h(x', y')|^2] dx dx' dy dy'. \quad (8)$$

After some algebra and using $\mathbb{E} [|u(x, y)|^2 |u(x', y')|^2] = 1 + c^2(x, y, x', y')$, (8) is written as

$$\begin{aligned} \mathbb{E} [\gamma_s^2] &= \frac{E_s^2 \beta^2}{\sigma^4} \left\{ \frac{\kappa^2 + 2\kappa}{(\kappa + 1)^2} W^2 H^2 + \frac{1}{(\kappa + 1)^2} \int_0^H \int_0^H \int_0^W \int_0^W \right. \\ &\quad \left[(1 + c^2(x, y, x', y')) + \kappa a(x, y) a^*(x', y') \mathbb{E} [u(x', y') u^*(x, y)] \right. \\ &\quad \left. + \kappa a^*(x, y) a(x', y') \mathbb{E} [u^*(x', y') u(x, y)] \right] dx dx' dy dy' \right\}. \end{aligned} \quad (9)$$

Using the first moment and the second moment in (9) followed by some algebra gives the variance as

$$\begin{aligned} \text{Var}[\gamma_s] &= \mathbb{E} [\gamma_s^2] - \frac{E_s^2 \beta^2 W^2 H^2}{\sigma^4} \\ &= \frac{E_s^2 \beta^2}{\sigma^4 (\kappa + 1)^2} \int_0^W \int_0^H \int_0^W \int_0^H c^2(x_1, y_1, x_2, y_2) dy_1 dx_1 dy_2 dx_2 \\ &\quad + \frac{2\kappa E_s^2 \beta^2}{\sigma^4 (\kappa + 1)^2} \text{Re} \left\{ \int_0^W \int_0^H \int_0^W \int_0^H a^*(x_1, y_1) a(x_2, y_2) \right. \\ &\quad \left. \times c(x_1, y_1, x_2, y_2) dy_1 dx_1 dy_2 dx_2 \right\}. \end{aligned} \quad (10)$$

Simplifying (10) requires a specific correlation model for the NLoS component of the channel. Here, we consider a correlation model that only depends on spatial separation, i.e., $c(x_1, y_1, x_2, y_2) = g(\sqrt{(x_2 - x_1)^2 + (y_2 - y_1)^2})$. The analysis below covers any correlation model of this kind. For numerical results, we adopt Clarke's model $g(x) = J_0(2\pi x / \lambda)$ where λ is wavelength and $J_k(\cdot)$ is the k-th order Bessel function. This is consistent with channel modeling for continuous antennas [7]. With this model, the first quadruple integral in (10) is given in our previous work [9].

We now compute the quadruple integral in the second term of (10). We denote the integrand by $\Omega(W, H)$ for convenience. The LoS signal at the continuous antenna is determined by θ and ϕ defined respectively as the elevation angle measured from the zenith and the azimuth angle measured from broadside. Hence, for an arbitrary point (x, y) on the antenna surface, the LoS component is given by $a(x, y) = e^{j(2\pi/\lambda)(y \sin \theta \sin \phi + x \cos \theta)}$. Thus, we calculate $\Omega(W, H)$ as

$$\begin{aligned} \Omega(W, H) &= \int_0^W \int_0^W \int_0^H \int_0^H e^{j(2\pi/\lambda)((y_2 - y_1) \sin \theta \sin \phi + (x_2 - x_1) \cos \theta)} \\ &\quad g(\sqrt{(x_2 - x_1)^2 + (y_2 - y_1)^2}) dy_1 dy_2 dx_1 dx_2. \end{aligned} \quad (11)$$

We use the change of variables $v = y_2 - y_1$, $s = x_2 - x_1$, $t = y_1$ and $u = x_1$ to rewrite (11) as

$$\Omega(W, H) = \int_{v=-W}^W (W - |v|) \int_{s=-H}^H (H - |s|) e^{j(mv+bs)} g(\sqrt{v^2 + s^2}) ds dv, \quad (12)$$

where $m = 2\pi \sin \theta \sin \phi / \lambda$ and $b = 2\pi \cos \theta / \lambda$. For the integral with respect to v , expressions $|v|$ and $g(\sqrt{v^2 + s^2})$ are even functions and $e^{j(mv)} = \cos(mv) + j \sin(mv)$ where $\sin(mv)$ is an odd function integrating to zero. Also, a similar observation can be made for the integral with respect to s . Hence, we rewrite (12) as

$$\begin{aligned} \Omega(W, H) &= \int_{v=-W}^W \int_{s=-H}^H (W - |v|)(H - |s|) \cos(mv) \cos(bs) \\ &\quad g(\sqrt{v^2 + s^2}) ds dv \\ &= 4 \int_{v=0}^W \int_{s=0}^H (W - v)(H - s) \cos(mv) \cos(bs) \\ &\quad g(\sqrt{v^2 + s^2}) ds dv. \end{aligned} \quad (13)$$

This reduces the quadruple integral in $\Omega(W, H)$ to the double integral in (13). Finally, the quadruple integral in the first term of $\text{Var}[\gamma_s]$ in (10) can be written in terms of single integrals using the results in our previous work [9]. Using these two techniques, the variance of the SNR is given by

$$\begin{aligned} \text{Var}[\gamma_s] &= \frac{4E_s^2 \beta^2}{\sigma^4 (\kappa + 1)^2} \left\{ \int_0^H r g^2(r) \left[WH \frac{\pi}{2} - (W+H)r + \frac{r^2}{2} \right] dr \right. \\ &\quad + \int_H^W r g^2(r) \left[WH \sin^{-1} \left(\frac{H}{r} \right) + W \sqrt{r^2 - H^2} - Wr - \frac{H^2}{2} \right] dr \\ &\quad - \int_W^{\sqrt{W^2 + H^2}} r g^2(r) \left[WH \left(\cos^{-1} \left(\frac{W}{r} \right) - \sin^{-1} \left(\frac{H}{r} \right) \right) \right. \\ &\quad \left. \left. + \frac{W^2 + H^2 + r^2}{2} - W \sqrt{r^2 - H^2} - H \sqrt{r^2 - W^2} \right] dr \right\} \\ &\quad + \frac{8\kappa E_s^2 \beta^2}{\sigma^4 (\kappa + 1)^2} \text{Re} \left\{ \int_{v=0}^W \int_{s=0}^H (W - v)(H - s) \cos(mv) \right. \\ &\quad \left. \cos(bs) g(\sqrt{v^2 + s^2}) ds dv \right\}. \end{aligned} \quad (14)$$

The integrals in (14) are easily computed with standard numerical methods as the integrands are smooth and bounded.

Using the mean and variance, our gamma approximation for γ_s is defined by $\gamma_s \sim G(\alpha, \delta)$ where $\alpha = (\mathbb{E}[\gamma_s])^2 / \text{Var}[\gamma_s]$ and $\delta = \mathbb{E}[\gamma_s] / \text{Var}[\gamma_s]$. The associated gamma probability density function (PDF) is denoted $p_{\gamma_s}(\gamma)$.

B. Achievable Rate: Upper Bound and Approximation

From Jensen's inequality, we have the simple upper bound:

$$\mathbb{E}\{R\} \leq R^{\text{up}} = \log(1 + \mathbb{E}\{\gamma_s\}) = \log(1 + E_s \beta W H / \sigma^2). \quad (15)$$

Next, using the approximated gamma distribution, $p_{\gamma_s}(\gamma)$, we derive the approximate mean of R as

$$\mathbb{E}\{R\} = \int_0^\infty \log_2(1 + \gamma) p_{\gamma_s}(\gamma) d\gamma. \quad (16)$$

Substituting the gamma PDF into (16) and changing base gives

$$\mathbb{E}\{R\} = \frac{\delta^\alpha}{\ln(2)\Gamma(\alpha)} \int_0^\infty \ln(1 + \gamma) \gamma^{\alpha-1} e^{-\delta\gamma} d\gamma, \quad (17)$$

where the gamma function is denoted by $\Gamma(\cdot)$. Finally, we express (17) using the Meijer G function $G(\cdot)$ [13]

$$\mathbb{E}\{R\} = \frac{1}{\ln(2)\Gamma(\alpha)} G_{3,2}^{1,3} \left(\begin{matrix} 1-\alpha & 1 & 1 \\ 1 & 0 & 1 \end{matrix} \middle| \frac{1}{\delta} \right), \quad (18)$$

where standard software packages are used to compute $G(\cdot)$.

C. Special Case: One-dimensional Continuous Antenna

Following a similar process as in Sec. III, we derive the SNR for a 1-D continuous antenna, by removing dimension y from the expressions. After MF, we have $\tilde{\eta} = \int_0^W |h(x)|^2 dx$. For the noise we can write $\mathbb{E}_n[|w|^2] = \sigma^2 \int_0^W |h(x)|^2 dx$. Thus, the instantaneous SNR for the 1-D case is

$$\tilde{\gamma}_s = \frac{E_s}{\sigma^2} \int_0^W |h(x)|^2 dx = \frac{E_s}{\sigma^2} \tilde{\eta}. \quad (19)$$

The first moment is $\mathbb{E}[\tilde{\gamma}_s] = \frac{E_s \beta W}{\sigma^2}$ since $\mathbb{E}[|h(x)|^2] = \beta$. Similar to the development of (8) and (9), we have

$$\begin{aligned} \text{Var}[\tilde{\gamma}_s] &= \frac{E_s^2 \beta^2}{\sigma^4 (\kappa + 1)^2} \int_0^W \int_0^W c^2(x, x') dx' dx \\ &\quad + \frac{2\kappa E_s^2 \beta^2}{\sigma^4 (\kappa + 1)^2} \text{Re} \left\{ \int_0^W \int_0^W a^*(x) a(x') c(x, x') dx' dx \right\}. \end{aligned} \quad (20)$$

In (20), we see that the $a(\cdot)$ functions in the second term are sinusoidal so that considerable cancellation occurs over the surface. Secondly, the first term contains squared correlations which tend to be small beyond a half-wavelength spacing. Hence, the integral has a small integrand over much of the integration region. As a result, the first term is also small relative to the mean SNR. The same trend occurs for the 2-D array, but it is harder to see the pattern due to the complexity of (14). Overall, the small variance relative to the mean shows that channel hardening is occurring.

For the NLoS component, we consider a correlation model that only depends on spatial separation, i.e., $c(x_1, x_2) = c_{1S}(|x_1 - x_2|)$. With this assumption we calculated the double integral in the first term of (20) in [9]. We now calculate the double integral in the second term of (20). Denote by $\tilde{\phi}$ the phase of the LoS signal as it hits the continuous antenna at point x' . Then we have $a(x') = e^{j\tilde{\phi}}$ and $a(x) = e^{j\tilde{\phi} + j2\pi(x' - x) \sin \tilde{\theta}}$ which gives $a^*(x) a(x') = e^{-j2\pi|x' - x| \sin \tilde{\theta}}$, where $\tilde{\theta}$ denotes the azimuth angle of the LoS signal measured from broadside. We calculate the double integral in the second term of (20) as

$$\begin{aligned} &\int_0^W \int_0^W e^{-j2\pi|x' - x| \sin \tilde{\theta}} c_{1S}(|x' - x|) dx' dx = \\ &2 \int_{x=0}^W \int_{x'=x}^W e^{-j2\pi(x' - x) \sin \tilde{\theta}} c_{1S}(x' - x) dx' dx. \end{aligned} \quad (21)$$

For the special case, $c_{1S}(x) = J_0(2\pi x / \lambda)$, we rewrite the expression in (21), after some algebra, as

$$2 \int_{t=0}^W (W - t) e^{-j2\pi t \sin \tilde{\theta}} J_0(2\pi t / \lambda) dt, \quad (22)$$

where $t = x' - x$. Therefore we have the second term of (20) using (22) and we use the results in [9] to compute the first

term of (20). Finally, we give the variance of $\tilde{\gamma}_s$ as follows:

$$\text{Var}[\tilde{\gamma}_s] = \frac{E_s^2 \beta^2}{\sigma^4 (\kappa + 1)^2} \left\{ 2W^2 {}_2F_3 \left(\frac{1}{2}, \frac{1}{2}; 1, 1, \frac{3}{2}; -(2\pi/\lambda)^2 W^2 \right) - W^2 J_1^2(2\pi W/\lambda) + 4\kappa \text{Re} \left[\int_{t=0}^W (W-t) e^{-j2\pi t \sin \bar{\theta}} J_0(2\pi t/\lambda) dt \right] \right\}, \quad (23)$$

where ${}_2F_3$ denotes the hypergeometric function. The single integral in (23) is easily computable with software. Finally, we can compute the shape and scale parameters of our gamma approximation for $\tilde{\gamma}_s$ using the mean and variance.

IV. NUMERICAL RESULTS

In this section, we show numerical examples to illustrate the accuracy of our derived approximations and to analyse the performance of continuous antenna systems. For simulations, the standard Riemann sum method is adopted to simulate the integral representations of γ_s and $\tilde{\gamma}_s$. Thus, the continuous antenna is divided into discrete points where the number of points is large enough so that the simulated integral converges. To have concise legends for the figures in this section, we use Sim. and Ana. in the legends as abbreviations for simulated and analytical results.

Figs. 1 and 2 show the cumulative distribution function (CDF) of the instantaneous received SNR, γ_s and $\tilde{\gamma}_s$ respectively, for a 2-D continuous surface and a 1-D continuous antenna, along with our approximated gamma distributions. The length of the 1-D continuous antenna and the area of the continuous surface antenna are fixed. Two frequencies 0.5 GHz and 28 GHz are used and the values in dB in the legend show the K-factor. As can be seen, our gamma approximations for both cases are excellent fits to the simulation across different frequencies and for different Rician K-factors.

For 28 GHz, with a smaller wavelength compared to 0.5 GHz, the spatial fading correlation in the NLoS component of the channel is smaller. Therefore, the channel values are less correlated, which leads to a better averaging over the continuous antenna and smaller SNR variation, making the CDFs more centered around the mean. Also, as seen for the larger Rician K-factor of 13 dB, the CDFs are more centered around the mean as the LoS component which is deterministic is stronger, resulting in smaller variances.

Fig. 3 shows the mean achievable rate and its upper bound obtained by simulations as well as our derived expressions in Sec. III-B. As seen, our approximation of the SNR leads to accurate achievable rate values. Also, the upper bound is almost exact for 28 GHz due to smaller spatial correlation and better averaging across the continuous antenna. Note that Jensen's inequality is tight for massive MIMO [14] and this property carries over to continuous antennas.

Fig. 4 shows the impact of changing the dimensions of a 2-D continuous antenna on the CDF of the SNR, when its area is fixed. From (7), the mean SNR is only a function of area, while (14) shows that the variance depends on both the width, W , and height, H , of the array. The figure shows that even if the area is fixed, changing the dimensions changes the distribution of the SNR due to the change in the variance. When the

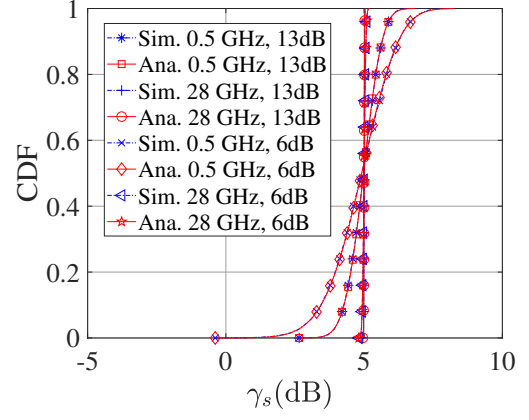


Fig. 1. CDF of SNR γ_s for a continuous surface antenna for $W = 600$ mm, $H = 400$ mm, $\theta = 40^\circ$, $\phi = 30^\circ$, with two values of κ shown in the legend in dB and $\beta E_s/\sigma^2$ is set so that $\mathbb{E}[\gamma_s] = 5$ dB.

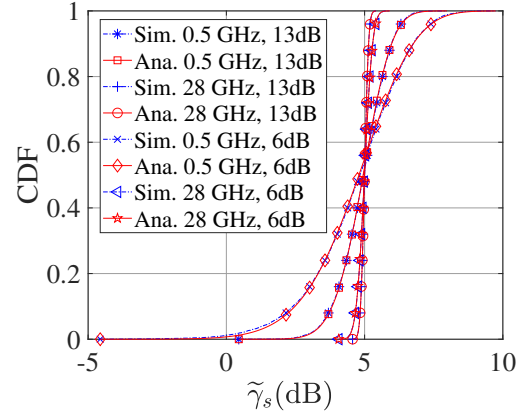


Fig. 2. CDF of SNR $\tilde{\gamma}_s$ for a 1-D continuous antenna and for a fixed length $W = 600$ mm, $\bar{\theta} = 40^\circ$, with two values of κ shown in the legend in dB and $\beta E_s/\sigma^2$ is set so that $\mathbb{E}[\tilde{\gamma}_s] = 5$ dB.

dimensions are changed, there are two effects. The first effect is that longer, thinner antennas have greater spacings and this causes more averaging of the scattered components and less variance. Hence, the CDF for $W = 4800$ mm, $H = 50$ mm, is sharper than the CDF when $W = 600$ mm, $H = 400$ mm. The second effect is due to the change in the LoS structure when the array dimensions are altered. This is more complex as the LoS components are sinusoidal and effects are not necessarily monotonic. This is seen in a comparison of the $W = 600$ mm, $H = 400$ mm layout and the $W = 300$ mm, $H = 800$ mm layout. The second layout is less compact and has greater spacings. Hence, the scattered part is averaged more, reducing the variance. However, the LoS effect dominates in this case and the variance is actually greater.

It is interesting to compare the performance of a traditional discrete array with the continuous antenna discussed here. Such a comparison is problematic as the typical model of an array is a set of discrete points with no area. Hence, a direct comparison will not compare like with like. For example, it will not correctly cater for the differences in channel correlations or captured energy. One could artificially scale the SNR of the channel for a discrete antenna array to make the received mean SNR equal to that of a continuous antenna. This compensates for the smaller captured energy by the discrete antenna array, so that any differences are due to

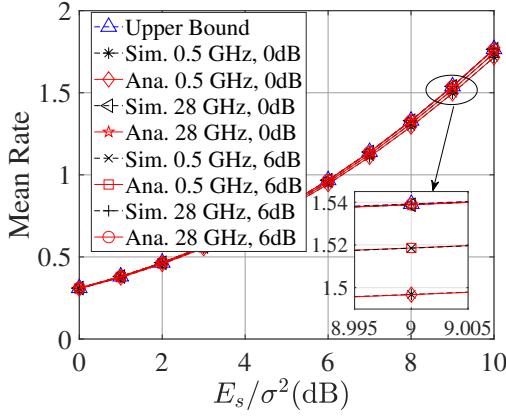


Fig. 3. Mean Rate for a continuous antenna for $\beta = 1$, $W = 600$ mm, $H = 400$ mm, $\theta = 40^\circ$ and $\phi = 30^\circ$. Also κ is shown in the legend in dB.

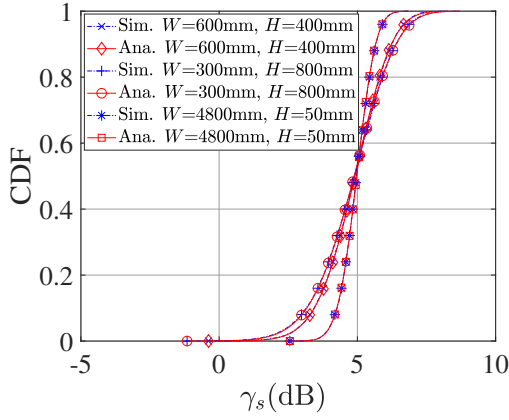


Fig. 4. SNR for a continuous antenna with a fixed aperture size, $\theta=40^\circ$, $\phi=30^\circ$, $\kappa=6$ dB, frequency 0.5 GHz and $\beta E_s/\sigma^2$ is set so that $\mathbb{E}[\gamma_s]=5$ dB.

the structure of the array rather than any power advantage. If this is done, the key advantage of the continuous array is in outage reduction. To understand this, note that a severe outage in a discrete array only requires the channel to be poor at a finite number of antenna positions. However, for a continuous array, a severe outage requires poor channels across the whole surface. This is much less likely and is the reason why continuous arrays have the property of removing outages.

Here, we propose an alternative, more consistent approach to such a comparison, where a single continuous antenna is compared to a square lattice of spatially separated sub-surfaces (each constituting a continuous antenna). In particular, Fig. 5 compares the CDFs of the SNR, γ_s , for a single 2-D continuous antenna and 4×4 and 8×8 sub-surface layouts that capture less energy as they are spatially separated. The total areas of the 4×4 and 8×8 layouts are respectively 69% and 44% of the area of the continuous antenna, giving a 1.58 dB and 3.52 dB drop in mean SNR which is proportional to total area. The dominant effect is simply the captured energy which shifts the CDFs. The effects on the shape of the distribution, for example through changes in variance, are very minor.

V. CONCLUSION

We derived gamma approximations for the distribution of the instantaneous received SNR for continuous antennas,

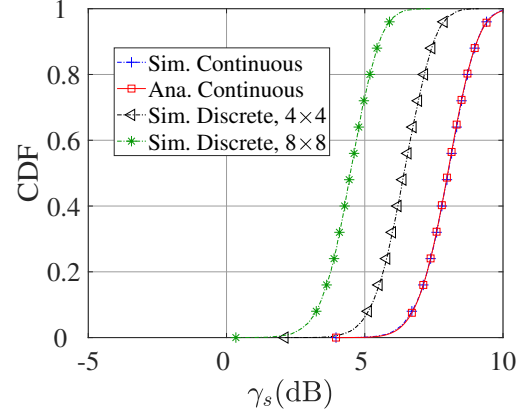


Fig. 5. CDF of SNR γ_s for a continuous antenna and discrete antenna arrays, for $W = 800$ mm, $H = 800$ mm, $\theta = 40^\circ$, $\phi = 30^\circ$, with $\kappa = 6$ dB, $\beta E_s/\sigma^2 = 10$ dB and frequency 0.5 GHz. The separation between sub-surfaces is half the width of each sub-surface of the 8×8 layout.

employing MF. We adopted a Rician channel model with a spatially correlated NLoS component. We also calculated an approximation for the mean achievable rate and provided its upper bound. Our numerical results for different frequencies and K-factors show that the SNR CDFs and rate approximations match simulated results in all cases to great accuracy.

REFERENCES

- [1] Z. Wan *et al.*, "Can continuous aperture MIMO obtain more mutual information than discrete MIMO?" *IEEE Commun. Lett.*, vol. 27, no. 12, pp. 3185–3189, Dec. 2023.
- [2] Z. Zhang *et al.*, "Pattern-division multiplexing for multi-user continuous-aperture MIMO," *IEEE J. Sel. Areas Commun.*, vol. 41, no. 8, pp. 2350–2366, Aug. 2023.
- [3] S. Hu *et al.*, "Beyond massive MIMO: The potential of data transmission with large intelligent surfaces," *IEEE Trans. Signal Process.*, vol. 66, no. 10, pp. 2746–2758, May 2018.
- [4] M. Jung *et al.*, "Performance analysis of large intelligent surfaces (LISs): Asymptotic data rate and channel hardening effects," *IEEE Trans. Wireless Commun.*, vol. 19, no. 3, pp. 2052–2065, Mar. 2020.
- [5] —, "Reliability analysis of large intelligent surfaces (LISs): Rate distribution and outage probability," *IEEE Wireless Commun. Lett.*, vol. 8, no. 6, pp. 1662–1666, Dec. 2019.
- [6] Ó. Martins *et al.*, "Achievable capacity for continuous radio stripe LOS communications," *IEEE Commun. Lett.*, vol. 27, no. 10, pp. 2792–2796, Oct. 2023.
- [7] A. Pizzo *et al.*, "Spatially-stationary model for holographic MIMO small-scale fading," *IEEE J. Sel. Areas Commun.*, vol. 38, no. 9, pp. 1964–1979, Sep. 2020.
- [8] X. Zhang *et al.*, "Fundamental limits of non-centered non-separable channels and their application in holographic MIMO communications," Feb. 2024. [Online]. Available: <https://arxiv.org/abs/2304.00223>
- [9] P. Smith *et al.*, "Continuous surface matched filtering: A finite dimensional analysis," in *Proc. 25th IEEE Wireless Commun. Netw. Conf. (WCNC)*, Dubai, United Arab Emirates, Apr. 2024, pp. 1–6.
- [10] N. K. Kundu *et al.*, "RIS-assisted MISO communication: Optimal beam-formers and performance analysis," in *Proc. IEEE Globecom Workshops*, Dec. 2020, pp. 1–6.
- [11] P. J. Smith *et al.*, "How accurate is your Gaussian/Gamma approximation?" *IEEE Wireless Commun. Lett.*, vol. 7, no. 5, pp. 804–807, Oct. 2018.
- [12] S. Atapattu *et al.*, "A mixture gamma distribution to model the SNR of wireless channels," *IEEE Transactions on Wireless Communications*, vol. 10, no. 12, pp. 4193–4203, Dec. 2011.
- [13] V. K. Dwivedi *et al.*, "A novel moment generating function based performance analysis over correlated Nakagami-m fading channels," *J. Comput. Electron.*, vol. 10, no. 4, p. 373381, Dec. 2011.
- [14] Q. Zhang *et al.*, "Power scaling of uplink massive MIMO systems with arbitrary-rank channel means," *IEEE J. Sel. Topics Signal Process.*, vol. 8, no. 5, pp. 966–981, Oct. 2014.